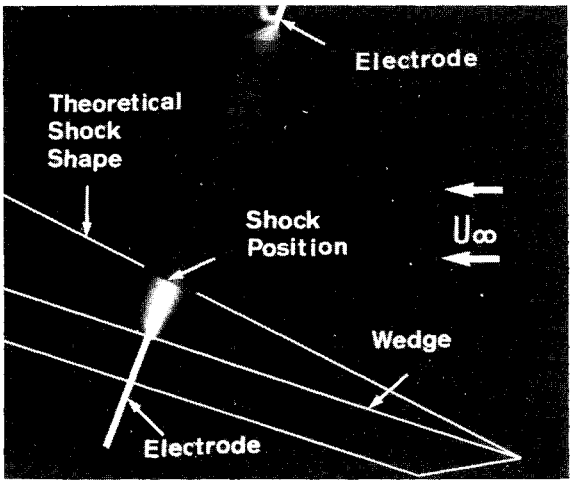

Fig. 4 Visualization of shock position over a wedge model.

minimum value is the decline of excitation functions after reaching the maximums, as mentioned before.

To verify the correctness of the above qualitative predictions, the relation between the value of the radiation intensity ratio I_∞/Is and the electric field E were investigated experimentally. In these experiments, shock waves were generated over a wedge. Electric discharges which cross the shock waves were generated under various electric fields and the electric discharge columns were photographed. From these discharge photographs, the radiation intensities I_∞ and Is at both parts just before and behind the shock waves were read with a sensitometer. Then, the radiation intensity ratio I_∞/Is was obtained. To read the radiation intensities at these parts of the discharge columns, a calibration curve was made in advance. The calibration curve was made as follows. The known intensities of light were applied to the films. The relative sensitization degree of these films was read with the sensitometer. Therefore, the relative radiation intensities from these parts of the discharge columns were obtainable by reading the sensitization degree at these parts with the sensitometer. These experiments were carried out when the molecular number density ratio N_∞/Ns was 1/3 and 1/5 by changing the angle of attack of the wedge. In these experiments, N_∞ was about 10^{17}/cm. The experimental results are shown in Fig. 3. It is shown that the qualitatively predicted I_∞/Is-curve vs the electric field agrees considerably with the results obtained experimentally.

In the case of $I_\infty/Is = 1$, the shock shape cannot be visualized since there exists no radiation contrast at the shock position. When the electric field is small enough, it seems to be suitable for the visualization of shock shapes since $I_\infty/Is \gg 1$ is realized. However, in order to generate an electric discharge under the condition of a small electric field, a great amount of electric current is required. Consequently, the flowfield would be disturbed and the visualization of shock shapes would not be successful. Therefore, it is best to select the electric field value at which the value of I_∞/Is is minimum.

The visualization of a shock wave generated over a wedge is demonstrated in Fig. 4. The characteristics of the hypersonic tunnel used in this experiment were as follows: Mach number is 10, static pressure is 1 mm Hg, flow duration is 10^{-2} s, and the diameter of the hypersonic nozzle exit is 0.15 m. The type of gas is air. The molecular number densities in the freestream and shock-wave layer are about $10^{17}/cm^3$ and $4.7 \times 10^{17}/cm^3$, respectively. A Nikon F camera is set just outside the observation window. The camera is set open during the experiment, and therefore the exposure time of the film is equivalent to the duration of the electric discharge itself. The film speed is ASA 1600. An electric discharge is generated while the hypersonic flow is obtained. The electric field in this experiment is about 150 V/cm. Concerning this electric discharge, the radiation intensity ratio I_∞/Is is about 1/5. The result indicates that the shock position is visualized exactly and clearly. The electric discharge can be photographed not only from the side, but also from the rear. Therefore, the present method can visualize three-dimensional shock shapes.

References

[1]Kimura, T., and Nishio, M., "Visualization of Shock Wave by Electric Discharge," *AIAA Journal*, Vol. 15, No. 5, 1977, pp. 611-612.

[2]Nasser, E., *Fundamentals of Gaseous Ionization and Plasma Electronics*, Wiley-Interscience, New York, 1970, pp. 74-75.

[3]Engel, V., *Ionized Gases*, Oxford Univ. Press, Oxford, England, UK, 1965, pp. 122-123.

Decoupling Approximation of Nonclassically Damped Structures

Steven Park,* Ilwhan Park,* and Fai Ma†
University of California, Berkeley,
Berkeley, California 94720

I. Introduction

In the analysis of a linear dynamic system, it is common practice to express the equations of motion in modal coordinates. If the resulting modal damping matrix is not diagonal, the system is said to be nonclassically damped. Because the existence of off-diagonal terms in the modal damping matrix complicates the analysis, the off-diagonal terms are usually ignored. This procedure is called the decoupling approximation. However, the off-diagonal terms can have significant influence on the response of a system, and ignoring the off-diagonal terms may cause substantial errors. An attempt to derive error bounds for the decoupling approximation has recently been reported by Shahruz and Ma[1] and by Hwang and Ma.[2] The purpose of this study is to present an exact analytical formula for the error and to illuminate the parameters that must be considered before the decoupling approximation can be applied to the equations of motion. For nonclassically damped linear systems subjected to harmonic excitations, three parameters in the equations of motion must be taken into consideration. The three parameters consist of the modal damping matrix, the natural frequencies, and the external excitation. The modal damping matrix and the natural frequencies are already known to be influential parameters, and their effect on the approximation error has been examined. We show in this Note that it is not adequate to consider just these two parameters. The interplay between all three parameters can lead to significant errors when invoking the decoupling approximation. Therefore, a proper study of the applicability of the decoupling approximation should include all three parameters.

A specific decoupling criterion based on just two parameters, the modal damping matrix and the natural frequencies, has been defined by Hasselman[3] and also by Warburton and Soni.[4] The criterion depends specifically on the amount of frequency separation between two natural frequencies, and it was asserted that adequate frequency separation between the modes is a sufficient condition for ignoring the off-diagonal terms of the modal damping matrix. It will be shown in this paper that frequency separation is not sufficient in insuring

Received June 4, 1991; revision received Jan. 17, 1992; accepted for publication Jan. 18, 1992.

*Research Assistant, Department of Mechanical Engineering.

†Associate Professor of Applied Mechanics, Department of Mechanical Engineering.

small errors. Instead of separating the natural frequencies, the excitation frequencies should be separated from the natural frequencies. This approach of frequency avoidance would prove to be more effective in reducing the errors introduced by the decoupling approximation.

II. Error Analysis

The equations of motion for an n degree-of-freedom linear dynamic system under external harmonic excitations can be represented as

$$M\ddot{x} + C\dot{x} + Kx = g(t), \quad x(0) = x_0, \quad \dot{x}(0) = \dot{x}_0, \quad t \geq 0 \tag{1}$$

where the mass matrix M, the damping matrix C, and the stiffness matrix K are of order $n \times n$. The displacement $x(t)$ and external harmonic excitation $g(t)$ are n-dimensional vectors. Applying the modal transformation $x(t) = Uq(t)$, the equations of motion become

$$\ddot{q} + \tilde{C}\dot{q} + \Omega^2 q = f(t), \qquad q(0) = U^T M x_0$$

$$\dot{q}(0) = U^T M \dot{x}_0, \qquad t \geq 0 \tag{2}$$

where U is the $n \times n$ modal matrix, $q(t)$ is the n-dimensional modal displacement vector, $U^TMU = I$ is the identity matrix, $U^TCU = \tilde{C}$ is the modal damping matrix, $U^TKU = \Omega^2$ is the diagonal matrix of eigenvalues, and $U^Tg(t) = f(t)$ is the n-dimensional modal excitation vector.

The decoupled equations of motion can be written as

$$\ddot{q}_a + \tilde{C}_d\dot{q}_a + \Omega^2 q_a = f(t), \quad q_a(0) = q_0, \quad \dot{q}_a(0) = \dot{q}_0, \quad t \geq 0 \tag{3}$$

where $\tilde{C}_d$ is a matrix composed of the diagonal elements of $\tilde{C}$, and $q_a(t)$ denotes the approximate solution vector.

Subtracting Eq. (3) from Eq. (2) and denoting the n-dimensional error vector as $e(t) = q(t) - q_a(t)$, we obtain

$$\ddot{e} + \tilde{C}_d\dot{e} + \Omega^2 e + \tilde{C}_r\dot{q} = 0, \qquad t \geq 0 \tag{4}$$

where $\tilde{C}_r$ is a matrix composed of the off-diagonal elements of $\tilde{C}$. Applying the Laplace transform to Eq. (4) for the initial conditions $q(0) = 0$ and $\dot{q}(0) = 0$, we have

$$E(s) = -(Is^2 + \tilde{C}_d s + \Omega^2)^{-1} s\tilde{C}_r Q(s) \tag{5}$$

where capital letters have been used to represent the Laplace transforms of the corresponding lower-case vectors. Substituting $Q(s) = (Is^2 + \tilde{C}s + \Omega^2)^{-1} F(s)$ in Eq. (5), we have

$$E(s) = -(Is^2 + \tilde{C}_d s + \Omega^2)^{-1} s\tilde{C}_r (Is^2 + \tilde{C}s + \Omega^2)^{-1} F(s) \tag{6}$$

The preceding equation is an analytical formula for the approximation error in the Laplace domain. This may be regarded as a quadrature solution of the approximation error, which can be obtained by taking the inverse Laplace transform. For the case of nonzero initial conditions, a corresponding expression of the approximation error can be derived in a similar fashion. Define the $n \times n$ transfer matrix by

$$H(s) = -(Is^2 + \tilde{C}_d s + \Omega^2)^{-1} s\tilde{C}_r (Is^2 + \tilde{C}s + \Omega^2)^{-1} \tag{7}$$

The ijth element of $H(s)$ can be expressed as the ratio of two polynomials,

$$H_{ij}(s) = \frac{a_0 s^m + a_1 s^{m-1} + \cdots + a_{m-1} s}{s^p + b_1 s^{p-1} + \cdots + b_p} \tag{8}$$

where a_i and b_i, in general, are nonzero constants. It can be shown by induction that

$$\frac{m}{p} = \begin{cases} \dfrac{2n-2}{2n+2} & \text{for } i = j \\ \dfrac{2n-3}{2n} & \text{for } i \neq j \end{cases} \tag{9}$$

At this point, two observations can be made about $H_{ij}(s)$. First, the denominator of $H_{ij}(s)$ is always of higher order than the numerator. Second, the denominator of $H_{ij}(s)$ has a nonzero constant term b_p, and the numerator does not have a coefficient for the s^0th term due to the multiplication by s in Eq. (6). Hence, the magnitude of $H_{ij}(s)$ approaches zero as s approaches zero and infinity. Therefore, there exists at least one local maximum for finite s in the transfer function. The highest peak, the number of peaks, and the shape of the transfer function are determined solely by the modal damping coefficients and the natural frequencies. This explains why these two parameters influence the approximation error.

From Eq. (6), it is evident that significant errors can be introduced by the covariation of the excitation with the transfer matrix. Both the excitation frequencies and the excitation amplitudes can affect the error. If we denote $s = i\omega_f$, the magnitude of $H_{ij}(s)$ ranges anywhere from zero to its highest value as ω_f varies. Thus, the excitation could also affect the value of $H_{ij}(s)$.

In many applications, the maximum approximation error is attained in the steady state. It has been mentioned that the interplay between the excitation, modal damping matrix, and natural frequencies can lead to significant errors of approximation. In the next section, a series of simulations will be used to demonstrate the effect of this interplay on the steady-state errors. An important observation will emerge: frequency separation is not sufficient to insure small errors when invoking the decoupling approximation.

III. Example and Discussion

Let us consider the equations of motion for the two-degree-of-freedom system

$$\begin{bmatrix} 1 & 0 \\ 0 & 1 \end{bmatrix} \begin{Bmatrix} \ddot{q}_1 \\ \ddot{q}_2 \end{Bmatrix} + \begin{bmatrix} c_{11} & c_{12} \\ c_{21} & c_{22} \end{bmatrix} \begin{Bmatrix} \dot{q}_1 \\ \dot{q}_2 \end{Bmatrix} + \begin{bmatrix} \omega_1^2 & 0 \\ 0 & \omega_2^2 \end{bmatrix} \begin{Bmatrix} q_1 \\ q_2 \end{Bmatrix} = \begin{Bmatrix} f_1(t) \\ f_2(t) \end{Bmatrix} \tag{10}$$

where $c_{12} = c_{21}$. To study the steady-state error, let $q(0) = 0$ and $\dot{q}(0) = 0$. For the first modal coordinate $q_1(t)$, the error in the Laplace domain is

$$E_1(s) = \left[\frac{c_{12}^2 s^2}{(s^2 + c_{11}s + \omega_1^2)(s^2 + c_{22}s + \omega_2^2) - (s^2 + c_{11}s + \omega_1^2)c_{12}c_{21}s^2} \right] F_1(s) + \left[\frac{-c_{12}s}{(s^2 + c_{11}s + \omega_1^2)(s^2 + c_{22}s + \omega_2^2) - c_{12}c_{21}s^2} \right] F_2(s) \tag{11}$$

where, consistent with Eq. (6), $F_1(s)$ and $F_2(s)$ are the Laplace transforms of $f_1(t)$ and $f_2(t)$, respectively. The error $e_1(t)$ can be obtained by taking the inverse Laplace transform of Eq. (11). To illustrate the influence of various parameters, we consider the steady-state amplitude of $e_1(t)$ for the following three cases:

$$\begin{bmatrix} 1 & 0 \\ 0 & 1 \end{bmatrix} \begin{Bmatrix} \ddot{q}_1 \\ \ddot{q}_2 \end{Bmatrix} + \begin{bmatrix} 2 & -0.1 \\ -0.1 & 1 \end{bmatrix} \begin{Bmatrix} \dot{q}_1 \\ \dot{q}_2 \end{Bmatrix} + \begin{bmatrix} \omega_1^2 & 0 \\ 0 & \omega_2^2 \end{bmatrix} \begin{Bmatrix} q_1 \\ q_2 \end{Bmatrix} = \begin{Bmatrix} 1 \sin 5t \\ 1 \sin 5t \end{Bmatrix} \tag{12}$$

$$\begin{bmatrix} 1 & 0 \\ 0 & 1 \end{bmatrix} \begin{Bmatrix} \ddot{q}_1 \\ \ddot{q}_2 \end{Bmatrix} + \begin{bmatrix} 2 & -0.2 \\ -0.2 & 1 \end{bmatrix} \begin{Bmatrix} \dot{q}_1 \\ \dot{q}_2 \end{Bmatrix} + \begin{bmatrix} \omega_1^2 & 0 \\ 0 & \omega_2^2 \end{bmatrix} \begin{Bmatrix} q_1 \\ q_2 \end{Bmatrix} = \begin{Bmatrix} 1 \sin 5t \\ 1 \sin 5t \end{Bmatrix} \tag{13}$$

$$\begin{bmatrix} 1 & 0 \\ 0 & 1 \end{bmatrix} \begin{Bmatrix} \ddot{q}_1 \\ \ddot{q}_2 \end{Bmatrix} + \begin{bmatrix} 2 & -0.1 \\ -0.1 & 1 \end{bmatrix} \begin{Bmatrix} \dot{q}_1 \\ \dot{q}_2 \end{Bmatrix} + \begin{bmatrix} \omega_1^2 & 0 \\ 0 & \omega_2^2 \end{bmatrix} \begin{Bmatrix} q_1 \\ q_2 \end{Bmatrix} = \begin{Bmatrix} 1 \sin 7t \\ 1 \sin 3t \end{Bmatrix} \tag{14}$$

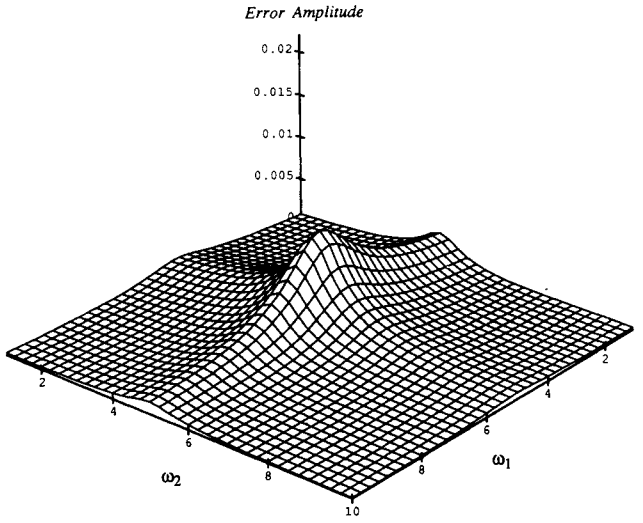

Fig. 1 Steady-state amplitude of $e_1(t)$ for Eq. (12); the control case.

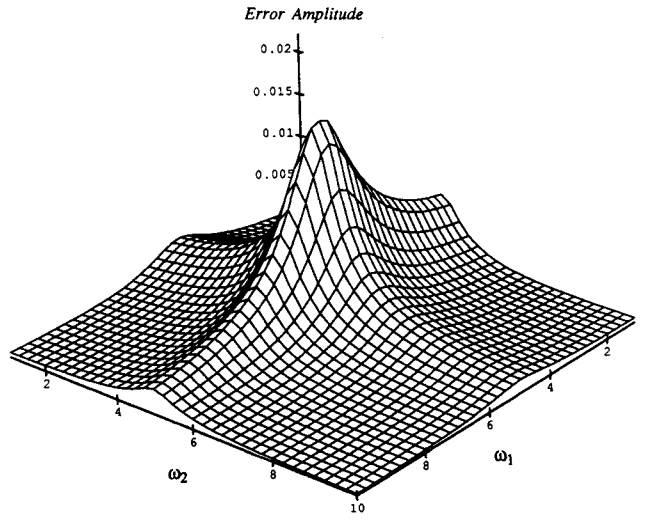

Fig. 2 Steady-state amplitude of $e_1(t)$ for Eq. (13).

Figure 1 represents the control case corresponding to Eq. (12), demonstrating the effect of varying the natural frequencies; this plot is qualitatively similar to Hasselman's plot of the degree of modal coupling. The maximum error in Fig. 1 occurs at a point along the diagonal $\omega_1 = \omega_2$ where the natural frequencies are close to the excitation frequency. The error is observed as having ridge-like characteristics. For higher-order systems, the error exhibits the same ridge-like characteristics when plotted against any two natural frequencies. Two ridges exist in Fig. 1; they run parallel to the ω_1 and ω_2 axes and lie along the frequencies of excitation. The peak error exists at the intersection of these two ridges, which also happens to be on the diagonal. The ridge along $\omega_1 = 5$ is less pronounced than the ridge along $\omega_2 = 5$ because $c_{11} > c_{22}$. In Fig. 2, the value of the off-diagonal damping elements has been doubled. The most obvious change is the overall increase in error magnitude. Besides this, the figure is qualitatively similar to the control case represented by Eq. (12). In Fig. 3, the values of the excitation frequencies have been changed. Compared with the control case, the peak error has now moved closer to $\omega_1 = \omega_2 = 3$, in addition to an increase in magnitude. Since most of the error in each of the three cases originates from $H_{12}(s)F_2(s)$, the second term in Eq. (11), the location of the peak mainly depends on the second excitation frequency. This explains the shifting of the peak found in Fig. 3. Another peak and a corresponding pair of ridges do exist from $H_{11}(s)F_1(s)$, but they are barely visible; this second peak is around $\omega_1 = \omega_2 = 7$. These figures demonstrate the effect of the interplay between the excitation, modal damping matrix, and natural frequencies on the approximation error. Higher-order systems exhibit similar qualitative features.

Hasselman[3] has stated that the decoupling approximation would not cause serious errors if there is adequate separation

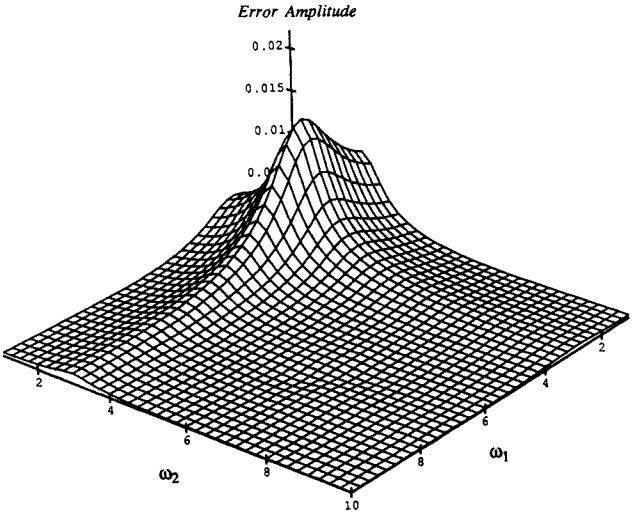

Fig. 3 Steady-state amplitude of $e_1(t)$ for Eq. (14).

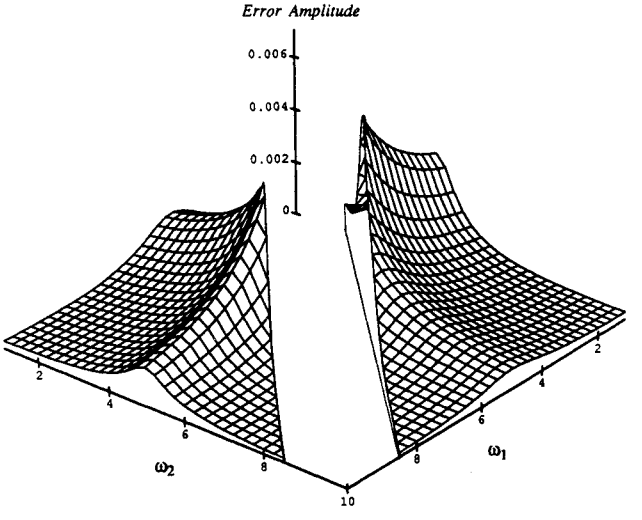

Fig. 4 Frequency separation applied to system (12).

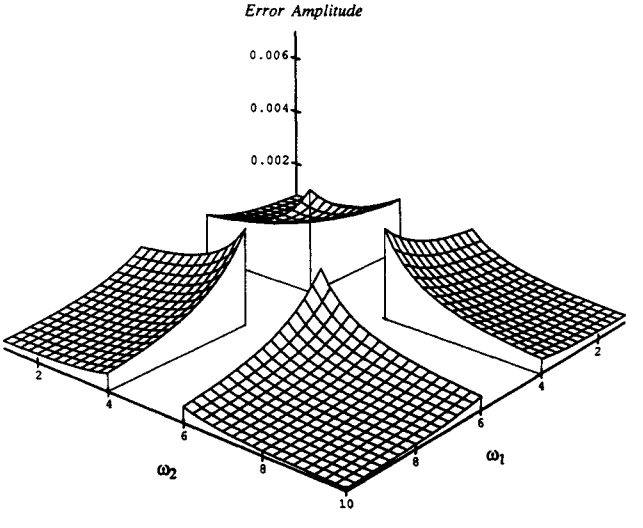

Fig. 5 Frequency avoidance applied to system (12).

between the natural frequencies. Separating the natural frequencies, in effect, removes a section along the diagonal $\omega_1 = \omega_2$, as shown in Fig. 4. This leaves behind much of the ridges that extend outward from the diagonal. However, the height of the ridges as seen in Fig. 1 is substantial. Small errors are therefore not insured by just removing a slice along the diagonal. Also, as seen in the figures, only a small portion along the diagonal—which contains the peak—needs to be removed. Instead of frequency separation, it would be more appropriate to remove or avoid regions near the excitation frequencies, as shown in Fig. 5. This approach of frequency avoidance addresses the ridge-like nature of the error. It would remove the ridges and the peak error, while allowing much of the diagonal region to remain intact. Although a limited set of data is presented in this paper, extensive numerical calculations have been performed by the author, and all numerical simulations have yielded qualitatively identical results.

IV. Conclusions

Given a system under harmonic excitation, the error introduced by the decoupling approximation depends on three parameters. They are the modal damping matrix, the natural frequencies, and the excitation. The approach of frequency separation is not adequate in insuring small errors. Instead, the approach of frequency avoidance provides a more effective method for controlling the error and, thus, for decoupling the system of equations. An analytical formula for the approximation error has also been presented to highlight the effect of the interplay of the three parameters on the approximation error.

Acknowledgment

This research has been supported in part by the National Science Foundation under Grant MSS-8657619. Opinions, findings, and conclusions expressed in this paper are those of the authors and do not necessarily reflect the views of the National Science Foundation.

References

[1]Shahruz, S. M., and Ma, F., "Approximation Decoupling of the Equations of Motion of Linear Underdamped Systems," *Journal of Applied Mechanics,* Vol. 55, No. 3, 1988, pp. 716–720.

[2]Hwang, J. H., and Ma, F., "On the Approximate Solution of Nonclassically Damped Linear Systems," *Journal of Applied Mechanics* (to be published).

[3]Hasselman, T. K., "Modal Coupling in Lightly Damped Structures," *AIAA Journal,* Vol. 14, No. 11, 1976, pp. 1627–1628.

[4]Warburton, G. B., and Soni, S. R., "Errors in Response Calculations for Non-Classically Damped Structures," *Earthquake Engineering and Structural Dynamics,* Vol. 5, No. 4, 1977, pp. 365–376.

Free Vibration Analysis of Rectangular Plates with Free Edges and Line Support Along Diagonals

Nong Li* and D. J. Gorman†
University of Ottawa,
Ottawa, Ontario K1N 6N5, Canada

Nomenclature

a,b	= dimensions of plate in ξ and η direction
D	= flexural rigidity of plate, $[Eh^3/12(1-\nu^2)]$
E	= Young's modulus of plate material
h	= thickness of plate
K^*	= upper subscript limit for first summations of solution
$W(\xi,\eta)$	= amplitude of plate vibration
x,y	= plate spatial coordinates
η	= dimensionless plate spatial coordinate, y/b
λ^2	$= \omega a^2\sqrt{\rho/D}$
λ^{*2}	$= \omega b^2\sqrt{\rho/D}$
ν	= Poisson's ratio
ξ	= dimensionless plate spatial coordinate, x/a
ρ	= mass of plate per unit area
ϕ	= plate aspect ratio, b/a
ϕ_1	= inverse of plate aspect ratio, a/b
ω	= circular frequency of vibration

Received Oct. 14, 1991; revision received Dec. 5, 1991; accepted for publication Dec. 6, 1991.

*Research Assistant, Department of Mechanical Engineering.
†Professor, Department of Mechanical Engineering.

Introduction

ALTHOUGH free vibration problems of free rectangular plates and plates with symmetrically distributed point supports on the lateral surface were investigated by Gorman,[1-3] where he used the superposition method to obtain analytical solutions, a review of the literature[4-6] reveals that no study has been made for the problem of free rectangular plates with line support along the diagonals.

It would seem that the title problem would be difficult to solve because of the existence of the line support. However, it will be seen that the superposition method can be utilized to obtain accurate solutions when the line support is replaced by a limited number of equally spaced point supports as described in this paper. Convergence tests show that only 20 point supports and 15 terms in series expansions are sufficient to guarantee rapid convergence to exact eigenvalues.

To save computing time and obtain rapid convergence, all of the vibration modes of this plate are placed in one of the following categories: fully symmetric, fully antisymmetric, or symmetric-antisymmetric modes with respect to the plate central axes. Eigenvalues are tabulated for the first four free vibration modes of plates with a wide range of plate geometries.

Mathematical Procedure

Consider the rectangular plate as shown in Fig. 1. The plate is of dimensions $2a \times 2b$ and has free edge conditions along all boundaries. In addition, the plate is subjected to internal line support along its diagonals, where lateral displacements are forbidden, but no bending moments normal to the line of support are imparted to the plate.

It is appreciated that the line support can be replaced by point supports, provided that the number of points are large enough to forbid lateral motion along the diagonals. This condition will be easily realized by imposing zero displacement at each of the points.

Since all modes must be symmetric with respect to the ξ and η axes and antisymmetric with respect to the ξ and η axes or symmetric with respect to the ξ (or η) axis and antisymmetric with respect to η (or ξ) axis, only one quarter of the plate needs

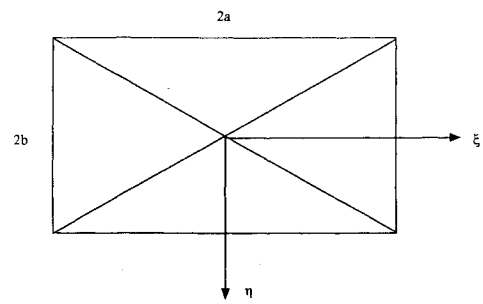

Fig. 1 Free rectangular plate subjected to internal line support along diagonals.